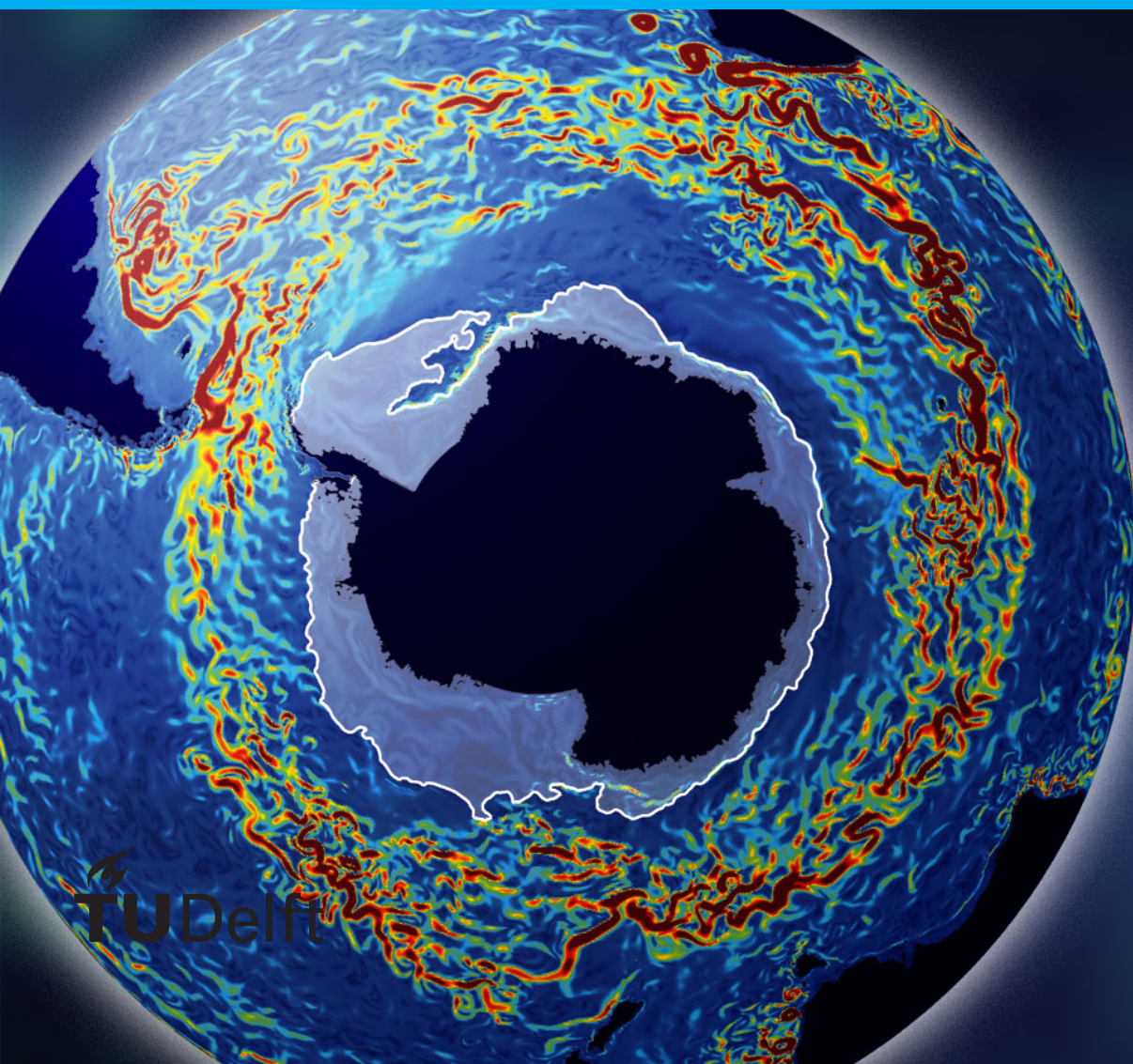# Mathematical model of the Antarctic Circumpolar Current with density variations

Analysing a boundary value problem modelling the Antarctic Circumpolar Current

T.A.B. Slavenburg

TUDelft

Mathematical model of the Antarctic Circumpolar Current with density variations

Analysing a boundary value problem modelling the Antarctic Circumpolar Current

by

T.A.B. Slavenburg

to obtain the degree of Bachelor of Science
at the Delft University of Technology,
to be defended publicly on Thursday July 3, 2025 at 15:00 PM.

An electronic version of this thesis is available at `http://repository.tudelft.nl/`.

TUDelft

Preface

"I would like to thank Dr. Kateryna Marynets for her guidance, insightful feedback, and continuous support throughout my bachelor project. I also like to thank Prof.dr. Dion Gijswijt for being part of my graduation committee."

Contents

List of Variables

t Radial coordinate (transformed)

$u(t)$ Stream function

$\varphi(t)$ Boundary interpolation function

$v(t)$ Shifted stream function

$f(u, t)$ Right-hand side of the differential equation

$F(u)$ Vorticity function

$\rho(u)$ Density function

$G(t, s)$ Green's function

ω Coriolis parameter

β Stratification parameter

ψ Original stream function before transformation

$\delta u(t)$ Perturbation of the stream function

r Stereographic radial coordinate

Ω Earth's angular velocity

R Earth's radius

r' Spherical radial coordinate

φ Longitude (spherical coordinate)

θ Latitude (spherical coordinate)

r Stereographic radial coordinate

ξ Stereographic complex coordinate

c Velocity scale for non-dimensionalisation

A, B Integration constants

L Growth bounds

N Lipschitz constants

T Operator in fixed-point reformulation

$\mathbb{R}$ Set of all real numbers

$\mathbb{R}^+$ Set of all strictly positive real numbers

C Space of continuous functions

C^1 Space of continuously differentiable functions

Laymen Summary

The Antarctic Circumpolar Current (ACC) is an important ocean current that flows all the way around Antarctica and influences our global climate. It can be seen as a fast, wide river in the ocean, driven by strong western winds and the Earth's rotation. The ACC keeps warm waters away from Antarctica, which helps to maintain the continent's cold environment [14].

To help understand how the ACC works, a simplified mathematical model, developed by the authors of [5], is used. The model captures how water flows around Antarctica and how variations in water density affect that flow. The model uses a single equation, called a stream function. The solution of this equation shows how strong the current is at different locations.

The results show that the strongest part of the current is somewhere in the middle, weakening near the boundaries. Changes in water density, like colder or saltier water, can influence the ocean's flow. The model behaves well with simple changes in density, but becomes unstable or unpredictable when the relationship is too strong or unrealistic. In those cases, small changes in input can lead to big differences in the outcome.

Modelling the ACC gives us insights into how rotation and density interact in shaping large-scale ocean currents. It helps scientists understand how the ACC might respond to future climate changes, especially when adding even more realistic features.

Summary

The Antarctic Circumpolar Current (ACC) is the only ocean current that flows continuously around the globe, and it plays a crucial role in global climate. It encircles Antarctica and keeps warm waters away, helping to maintain the continent's cold environment [14]. This report studies a simplified mathematical model to capture the ACC's steady-state behaviour, incorporating the effects of density stratification.

The model studied is originally developed by Ding in [5], who reformulated the ocean dynamics of Arctic gyres as a non-linear boundary value problem (BVP). Their approach uses shallow-water equations, developed by Johnson and Constantin in [4], combined with a stereographic projection to reduce the spherical geometry to a planar coordinate system. This leads to a second-order non-linear differential equation for a stream function $u(t)$ that describes the flow field. This includes the effect of Earth's rotation (Coriolis effect), represented by ω, a prescribed vorticity distribution $F(u)$, and a stratified density function $\rho(u)$.

In this report, the model in [5] is adapted to describe the ACC. This is achieved by imposing Dirichlet boundary conditions representing the two latitudinal limits. This leads to a BVP defined on a finite domain, providing an appropriate mathematical framework for capturing the flow of the ACC.

After simplifying the differential equation to an integral equation, our analytical analysis of the model showed that under reasonable assumptions, an unique solution exists. Before computing a numerical solution, the assumptions introduced in the analytic analysis were verified for the specific choices of F and ρ, confirming their regularity and positivity. The equation was then solved numerically using a collocation method, yielding a stream function profile, consistent with observed ACC behaviour. The numerical solution was validated against an exact solution in a special case (constant F and ρ), showing excellent agreement (error $< 10^{-6}$). Stability tests confirmed that the solution changes only slightly under small perturbations in boundary conditions.

Finally, the influence of different density stratification profiles was explored. Gentle stratification (constant or linear $\rho(u)$) led to a stable, symmetric jet, whereas strongly non-linear stratification (quadratic or exponential $\rho(u)$) resulted in oscillatory or unstable solutions. This highlights the model's sensitivity to stratification.

In summary, this report has shown that a mathematically rigorous and physically consistent model for the ACC can be analysed and solved with a non-linear differential equation. The theoretical contributions are complemented by numerical results that validate the model's applicability, providing a strong basis for further exploration of large-scale ocean dynamics.

1

Introduction

The Antarctic Circumpolar Current (ACC) plays a significant role in global ocean circulation. Of all major currents, it is the only one that circulates continuously around the globe without any interruption of land. The ACC flows eastward (clockwise direction) around Antarctica, and it passes through the Atlantic, Pacific, and Indian Oceans. The flow is primarily driven by westerly winds and the Coriolis effect, which is a consequence of Earth's rotation. With a length of approximately 24,000 km and a width up to 2000 km [9], the ACC plays a crucial role in controlling global climate, as it facilitates the exchange of water between ocean basins. This causes the formation of a thermal barrier that shields Antarctica from warmer subtropical water, helping to maintain the continent's cold environment [14].

Modelling and understanding the dynamics of large ocean gyres and currents is important in science and oceanography. Ocean currents such as the ACC transport mass, heat, salt, and nutrients across oceans, which directly influences sea level, ecosystems, and the global carbon cycle. From a mathematical perspective, currents and gyres provide valuable insights into how rotation and density differences shape the internal dynamics and forcing of large-scale ocean flows.

This report aims to explore a simplified mathematical model of the ACC, adapted from a model developed by Ding [5] for stratified Arctic gyres. Their model, obtained from the shallow-water equations on a rotating sphere [4], reduces to a second-order non-linear differential equation in a radial coordinate after applying the stereographic projection. This results in a boundary value problem (BVP) for the stream function u and includes the Coriolis effect, represented by ω, a prescribed vorticity distribution F, and a stratified density function ρ.

The BVP is modified to reflect the appropriate domain and boundary conditions for the ACC. The studied model is considered on a finite radial interval with Dirichlet boundary conditions, which assume that the flow vanishes at the edges of the current. This reflects the physical assumption that the ACC is bounded between two latitudinal limits. To understand the mathematical behaviour of the system, the model is studied through both analytical and numerical methods. The real analysis part focuses on proving existence and uniqueness results under broad conditions. A numerical solution is found through a collocation method, and is compared to an analytic solution. Then, different forms of the density functions are explored to assess how this affects the stream function u of the ACC.

This report is structured as follows. The second chapter introduces the mathematical model and provides the physical and theoretical background. Chapter 3 gives a simplified version of the model and shows existence and uniqueness results for the BVP. Chapter 4 presents a numerical solution of the model and provides a numerical analysis of its behaviour. The final chapter is devoted to conclusions and discussions, including a summary of the results, with suggestions for further research.

2

Background

In this chapter, the theoretical and mathematical background of the model studied in this report is discussed. The first section introduces the physical context of gyres and currents. Then, the origin of the model developed in [5] is outlined. The last section describes how this model is adapted to represent the ACC.

2.1. Physical Background

This section reviews the structure and dynamics of ocean gyres and currents, and the impact of Coriolis force and density stratification in shaping large-scale geophysical flows. These mechanisms motivate the modelling assumptions used in the derivation of the model in the following section.

A gyre is a large system of rotating ocean currents. More specifically, ocean gyres are large-scale, slowly evolving circulation systems mainly driven by wind forcing and planetary rotation (Coriolis force). They typically develop in ocean basins and exhibit stable, large-scale circulation patterns. Five major subtropical gyres dominate the world's oceans, such as the North Atlantic and North Pacific gyres, see Figure 2.1.
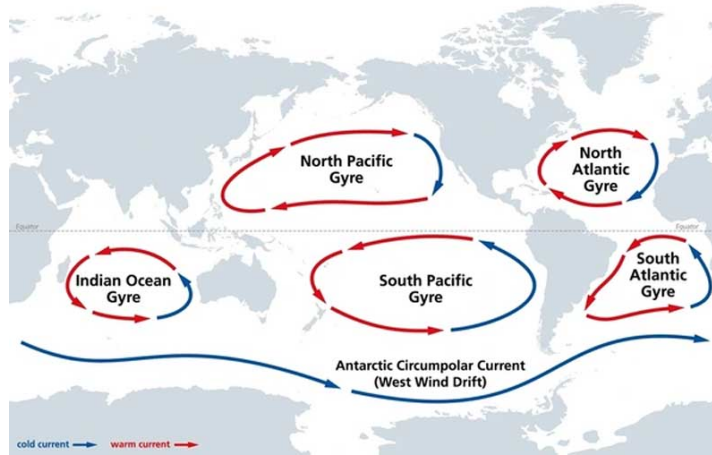

Figure 2.1: Global ocean circulation showing the five major gyres and the ACC [6].

These systems play a crucial role in transporting heat, sustaining marine ecosystems, and influencing large-scale climate dynamics [18]. In contrast to the subtropical gyres, Arctic gyres form nearly closed circulations around the polar area and exhibit radial symmetry and steady behaviour. This makes them suitable for mathematical modelling. The model in [5] is originally developed to describe Arctic gyres. Starting from the inviscid Euler equations on a rotating sphere, a non-linear BVP is formulated. The model captures the effects of vorticity, stratification, and rotation. Although designed for a polar setting, mathematical structure of the model also applies to other large-scale flows. The ACC shares key physical characteristics such as rotational influence, stratification, and latitudinal confinement. This motivates modelling the ACC by adapting the model for Arctic gyres, forming the basis for the analysis in this report.

The Coriolis force is a pseudo force that arises when observing motion from a rotating reference frame, such as the Earth. It describes the deflection of moving objects relative to Earth's surface, caused by the planet's rotation. As a result, moving water experiences a deflection to the right in the Northern Hemisphere and to the left in the Southern Hemisphere. This mechanism contributes to the circular motion of gyres and the zonal structure of currents like the ACC. This is called the Coriolis effect [11]. In the governing equations, introduced in the next section, the Coriolis force appears as $2\Omega \times \mathbf{v}$, with Ω representing Earth's angular velocity and $\mathbf{v}$ the fluid velocity. In reduced models, this influence is defined by the parameter ω, which quantifies the strength of rotation. This report uses $\omega \approx 4650$ as the value of the non-dimensionlised form of the Coriolis parameter.

In oceanography, stratification typically refers to the vertical variation in ocean density, caused by differences in temperature and salinity. This creates distinct layers and stabilizes the horizontal flow by resisting vertical motion. In mathematical models [15], stratification is often represented by a density function $\rho = \rho(\psi)$, which links density to the stream function. Instead of using vertical layers, the fluid is modelled as a two-dimensional system where the density changes across the flow and depends on the flow pattern. In the reduced model, the density ρ and its derivative appear in the governing equation, linking the flow and density through non-linear terms. Such terms are necessary to capture how rotation and density variation shape the structure of flows like the ACC.

2.2. Origin of the model

This section outlines some mathematical techniques and explains how they are used in the derivation of the model in [5]. Rather than presenting every step in detail, the aim is to get a clear understanding of how each mathematical technique helps to reduce governing equations to the final equation used in this report. First, the Euler equations for rotating, stratified flow on a sphere are described. Then, the shallow-water approximation and the concept of stream function and vorticity are explained. Finally, the use of stereographic projection and coordinate transformation are introduced that lead to final BVP.

2.2.1. Governing Equations on the Rotating Sphere

The model in [5] is based on the incompressible, inviscid Euler equations for stratified flow on a rotating sphere. These equations describe the dynamics of a fluid layer under the influence of pressure gradients, gravity, and Earth's rotation. The spherical coordinates used are (φ, θ, r'), where $\varphi \in [-\pi, \pi)$ denotes longitude, $\theta \in \left(-\frac{\pi}{2}, \frac{\pi}{2}\right)$ is the latitude, and r' is the radial distance from the centre of the Earth. In Figure 2.2, φ and θ are visualised, and r' is represented by the distance from the centre of the Earth to point P.
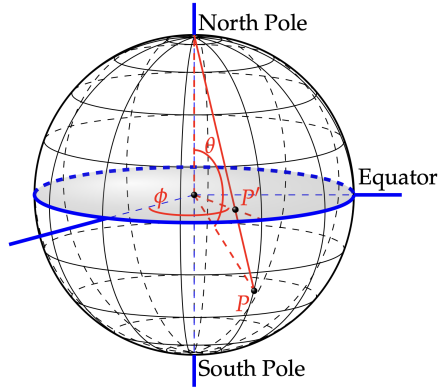
Figure 2.2: Stereographic projection from the North Pole to the equatorial plane.[7]

The Euler equations take the form

$$\frac{D\mathbf{u}'}{Dt'} + 2\mathbf{\Omega}' \times \mathbf{u}' = -\frac{1}{\rho'}\nabla p' + \mathbf{g}', \tag{2.1}$$

where $\mathbf{u}' = (u', v', w')$ is the velocity field consisting of the zonal, meridional, and vertical components, respectively, ρ' is the ocean water density, p' the pressure, $\mathbf{\Omega}'$ the angular velocity vector of the Earth, and $\mathbf{g}'$

the gravitational acceleration. The gradient $\nabla p'$ describes how pressure changes with position. This formulation is expressed in physical coordinates on the rotating sphere, where the velocity, pressure, and density represent three-dimensional physical fields.

The fluid is assumed to be incompressible, which gives us the mass conservation condition

$$\nabla \cdot \mathbf{u}' = 0. \tag{2.2}$$

Here, $\nabla \cdot \mathbf{u}'$ expresses the divergence of the velocity field, representing volume conservation at each point in the fluid.

In addition, as the fluid is stratified, this gives the incompressibility condition

$$\frac{D\rho'}{Dt'} = 0, \tag{2.3}$$

which states that the density of a fluid parcel does not change as it moves through the flow. Under the assumptions of axisymmetry and steady flow, the density can be defined as a function of the stream function, introduced later in this section: $\rho' = \rho(\psi)$. This allows the model to include baroclinic effects in a simplified but physically meaningful way. To simplify the analysis, several standard assumptions are made. The flow is assumed to be steady (no time dependence), purely horizontal (neglecting vertical motion), and axisymmetric (no dependence on longitude). These assumptions reduce the full three-dimensional equations to a lower-dimensional system.

2.2.2. Shallow-Water Approximation

To simplify the governing equations, the authors in [5] apply the shallow-water approximation. This assumes that the vertical scale of the fluid layer is much smaller than the horizontal scale, which is appropriate for large-scale ocean flows such as the Arctic gyres and the ACC.

The vertical coordinate r' is then written as

$$r' = R' + H'z, \tag{2.4}$$

where H' is the mean depth of the ocean (typically $H' \approx 4\,\mathrm{km}$), R' the Earth's mean and $z \in [-1,0]$ is a scaled vertical coordinate [4, 5]. Using this new coordinate, a rescaled stream function is defined:

$$\psi'(\theta, r') = H'R'\psi(\theta, z), \tag{2.5}$$

where ψ is a dimensionless function depending on latitude and vertical coordinate. This accounts for the curvature of the Earth and the ocean layer thickness.

2.2.3. Stream Function and Vorticity

In fluid dynamics, stream functions are often used to describe incompressible, two-dimensional flow. Instead of working with all velocity components, the flow can be represented by a single scalar function. Also, using a stream function ensures the mass conservation condition automatically. This makes the equations easier to work with, especially when the flow is steady and symmetric, like in Arctic gyres and the ACC.

The stream function ψ is introduced so that the horizontal velocity can be expressed in terms of derivatives of ψ. Under axisymmetry, only the zonal (east-west) velocity remains and becomes

$$v_\varphi = \frac{1}{\rho \, r'} \frac{\partial \psi}{\partial \theta}. \tag{2.6}$$

This representation also allows the vorticity to be written in terms of ψ, which simplifies the equations.

In the model, the stream function combines the effects of rotation and density variation in one function, and helps reduce the full system to a simpler form.

2.2.4. Stereographic projection

Stereographic projection is a classical method for mapping the surface of a sphere onto a plane. It is angle-preserving and transforms circles of latitude into circles or straight lines in the plane. This property makes it especially useful for simplifying models on a rotating sphere.[7]

In this setting, the stereographic projection from the North Pole onto the equatorial plane is considered, as shown in Figure 2.2. A point P' on the equatorial plane is obtained as a result of the stereographic projection

of a point P from the North Pole. Under this projection, the entire southern hemisphere is mapped onto the equatorial plane.

This projection is expressed using a complex coordinate

$$\xi = \frac{\cos\theta}{1+\sin\theta}e^{i\varphi}, \tag{2.7}$$

with the radial coordinate in the plane given by

$$r = |\xi| = \frac{\cos\theta}{1+\sin\theta}. \tag{2.8}$$

The projection simplifies the mathematical form of differential operators, such as the Laplacian and vorticity, and transforms the geometry into a symmetric system in r. This leads to a reduced equation for the stream function ψ in planar Cartesian coordinates (x, y), as given in [5]:

$$\Delta\psi + 8\omega\frac{\sqrt{\rho(\psi)}(1-x^2-y^2)}{(1+x^2+y^2)^3} + 2\omega^2\frac{\rho'(\psi)(1-x^2-y^2)^2}{(1+x^2+y^2)^4} - \frac{4F(\psi)}{(1+x^2+y^2)^2} = 0, \tag{2.9}$$

where $F:\mathbb{R}\to\mathbb{R}$ is a arbitrary smooth vorticity function and $\rho:\mathbb{R}\to\mathbb{R}^+$ is a strictly positive density, continuously differentiable function.

2.2.5. Final Reduced Model

To further reduce the equation (2.9) derived in the planar domain, lastly the authors of [5] introduce a change of variables, the stereographic radial coordinate r is transformed

$$t = -\log r,$$

so that large values of t correspond to small distances from the origin in the plane (to regions close to the pole on the sphere). This transformation maps the unbounded domain $r \in (0,\infty)$ onto the real line $t \in (-\infty,\infty)$. In practice, the physically relevant region lies in the range $t \in [t_0,\infty)$, where the reduced model is defined.

After substituting the stream function $u(t) = \psi(r(t))$ into (2.9), the model reduces to the following second-order ordinary differential equation:

$$u''(t) = \frac{F(u(t))}{\cosh^2 t} - 2\omega\frac{\sinh t}{\cosh^3 t}\sqrt{\rho(u(t))} - \frac{\omega^2\rho'(u(t))\sinh^2 t}{2\cosh^4 t}, \quad t > t_0. \tag{2.10}$$

This simplified equation incorporates three main physical components: the prescribed vorticity $F(u)$, the effect of planetary rotation scaled by a constant ω, and the contribution of density stratification through the function $\rho(u)$.

In this model, the domain is taken as $t \in [t_0,\infty)$, and asymptotic boundary conditions are imposed:

$$\lim_{t\to\infty} u(t) = \psi_0, \qquad \lim_{t\to\infty} u'(t)\cosh t = 0. \tag{2.11}$$

This BVP serves as the starting point for the adaptation to the ACC, which is carried out in the next section.

2.3. Adaptation to the ACC Setting

The reduced equation (2.10) was originally formulated for Arctic gyres, which exhibit a closed, radially symmetric structure. In contrast, the ACC forms an open, zonal flow band around Antarctica, bounded by two latitudinal limits. To account for this difference, the domain is changed to a finite interval $t \in [t_1, t_2]$, where $t = -\log r$ is the transformed radial coordinate introduced earlier. The values t_1 and t_2 correspond to the inner and outer boundaries of the current, illustrated in Figure 2.3.
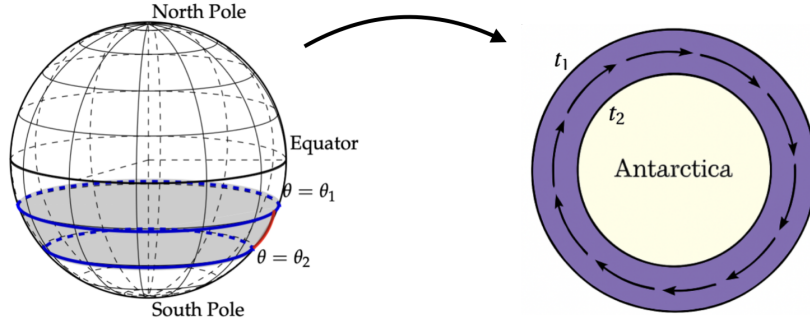
Figure 2.3: Stereographic projection of the ACC band onto a planar annulus [7].

This gives

$$u''(t) = \frac{F(u(t))}{\cosh^2 t} - 2\omega \frac{\sinh t}{\cosh^3 t} \sqrt{\rho(u(t))} - \frac{\omega^2 \rho'(u(t)) \sinh^2 t}{2 \cosh^4 t}, \qquad t \in [t_1, t_2]. \tag{2.12}$$

Also the boundary conditions (2.11) must be adapted. It is chosen to impose Dirichlet conditions at both endpoints. In this report, two variants are considered. The first is the homogeneous case

$$u(t_1) = u(t_2) = 0, \tag{2.13}$$

which may be interpreted as a current enclosed between two streamlines where $u(t) = 0$ outside of those streamlines. The second is the non-homogeneous case

$$u(t_1) = \alpha_1, \quad u(t_2) = \alpha_2, \tag{2.14}$$

where the difference $\alpha_2 - \alpha_1$ reflects the net volume transport across the current.

These modifications define the adapted version of the model used throughout the remainder of this report. While the domain and boundary conditions differ from those in the original setting, the mathematical structure of the equation remains unchanged.

3

Analytic Results

In this chapter, the existence and uniqueness of solutions to equation (2.12) with boundary conditions (2.13) and (2.14) are studied. The first part gives a simplification of the non-linear differential equation (2.12) to an integral equation. The sections after give a proof of existence using a variation of Schauder's fixed theorem, and a uniqueness result under suitable Lipschitz assumptions.

3.1. Simplification of the model

To analyse the mathematical properties of the model, the differential equation (2.12) is reformulated. This reformulation will allow us to prove existence and uniqueness results. First, the integral formulation for the homogeneous Dirichlet boundary conditions (2.13) is presented, and then it is extended to the non-homogeneous case (2.14).

Consider the non-linear second-order differential equation:

$$u''(t) = f(u(t), t), \tag{3.1}$$

on a closed interval $[t_1, t_2] \subset \mathbb{R}$, where the function $f(u(t), t)$ is defined by

$$f(u(t), t) = \frac{F(u)}{\cosh^2 t} - 2\omega \frac{\sinh t}{\cosh^3 t} \sqrt{\rho(u)} - \frac{\omega^2 \rho'(u) \sinh^2 t}{2 \cosh^4 t}, \tag{3.2}$$

where $F : \mathbb{R} \to \mathbb{R}$ is a arbitrary smooth vorticity function, $\rho : \mathbb{R} \to \mathbb{R}^+$ is a strictly positive, continuously differentiable density function and $u : [t_1, t_2] \to \mathbb{R}$ is a twice continuously differentiable stream function.

3.1.1. Homogeneous Dirichlet boundary conditions

First, consider the case where $u(t)$ satisfies the homogeneous boundary conditions (2.13). For this BVP, the linear differential operator $\mathscr{L}[u] = u''(t)$ with (2.13) is studied. The corresponding Green's function $G(t, s)$ for this operator is given by:

$$G(t, s) = \begin{cases} \frac{(t-t_1)(t_2-s)}{t_2-t_1}, & t \le s, \\ \frac{(s-t_1)(t_2-t)}{t_2-t_1}, & s < t. \end{cases} \tag{3.3}$$

It satisfies $G(t_1, s) = G(t_2, s) = 0$ for all s, and is symmetric: $G(t, s) = G(s, t)$.

Using this Green's function, any solution $u(t) \in C^2([t_1, t_2])$ of the homogeneous BVP satisfies the integral equation:

$$u(t) = \int_{t_1}^{t_2} G(t, s) f(u(s), s) \, ds. \tag{3.4}$$

This reformulation transforms the BVP into an equivalent integral equation, which is more suitable for proving existence and uniqueness results. Next, this formulation is adapted to the case of non-homogeneous Dirichlet boundary conditions.

3.1.2. Non-homogeneous Dirichlet boundary conditions

In many physical settings, including the ACC, the stream function does not necessarily vanish at the boundaries. Instead, the boundary conditions take the form (2.14). To reduce the problem to one with homogeneous boundary conditions, an affine function $\varphi(t)$ is introduced such that:

$$\varphi(t_1) = \alpha_1, \quad \varphi(t_2) = \alpha_2, \tag{3.5}$$

with:

$$\varphi(t) = \alpha_1 + \frac{t - t_1}{t_2 - t_1}(\alpha_2 - \alpha_1). \tag{3.6}$$

Define $v(t) = u(t) - \varphi(t)$, so that $v(t_1) = v(t_2) = 0$, and rewrite the differential equation as:

$$v''(t) = f(v(t) + \varphi(t), t). \tag{3.7}$$

Then, using the same Green's function as in the homogeneous case, $v(t)$ satisfies the integral equation:

$$v(t) = \int_{t_1}^{t_2} G(t, s) f(v(s) + \varphi(s), s) \, ds, \tag{3.8}$$

and the solution of the non-homogeneous BVP satisfies:

$$u(t) = \varphi(t) + \int_{t_1}^{t_2} G(t, s) f(u(s), s) \, ds. \tag{3.9}$$

This integral formulation will form the basis for the existence proof in the next section.

3.2. Existence of a solution

In this section the existence of a solution of equation (2.12) with boundary conditions (2.14) is proven.

Theorem 3.1

Let $F : \mathbb{R} \to \mathbb{R}$ and $\rho : \mathbb{R} \to \mathbb{R}^+$ in equation (2.12) *be continuous functions satisfying the following conditions*:

- *There exist constants $\rho_{\min} > 0$ and $\rho_{\max} < \infty$ such that*

$$\rho_{\min} \leq \rho(u) \leq \rho_{\max} \quad \text{for all } u \in \mathbb{R}. \tag{3.10}$$

- *F has at most linear growth:*
$$|F(u)| \leq L_F(1 + |u|) \quad \text{for some } L_F > 0. \tag{3.11}$$

- *ρ is continuously differentiable and*

$$|\rho'(u)| \leq L_{\rho'} \quad \text{and} \quad |\sqrt{\rho(u)}| \leq L_\rho \quad \text{for all } u \in \mathbb{R}. \tag{3.12}$$

Then there exists at least one function $v \in C^2([t_1, t_2])$ that satisfies the equation (3.7) *and boundary conditions $v(t_1) = v(t_2) = 0$. Let $\varphi(t)$ be as in* (3.6)*, satisfying* (3.5)*. Consequently, $u(t) = v(t) + \varphi(t)$ is a solution of the original problem* (2.12) *with boundary conditions* (2.14)*.*

Proof

Let $X := \{v \in C^2([t_1, t_2]) : v(t_1) = v(t_2) = 0\}$ be the closed subspace of the Banach space $C([t_1, t_2])$, equipped with supremum norm $\|v\|_\infty := \max_{t \in [t_1, t_2]} |v(t)|$.

Define the operator

$$(Tv)(t) := \int_{t_1}^{t_2} G(t, s) f(v(s) + \varphi(s), s) \, ds.$$

Then $u = v + \varphi$ solves the original problem if and only if $v = Tv$.

Let

$$K := \{v \in C^2([t_1, t_2]) : \|v\|_\infty \leq M\}$$

be the closed ball for some $M > 0$. Using the bounds on F, ρ, and ρ', given in (3.10)-(3.12) first the estimate is found for:

$$|f(v(t)+\varphi(t),t)| \leq \frac{L_F(1+|v(t)+\varphi(t)|)}{\cosh^2 t} + 2\omega\frac{\sqrt{\rho_{\max}}|\sinh t|}{\cosh^3 t} + \frac{\omega^2 L_{\rho'}\sinh^2 t}{2\cosh^4 t}.$$

Note, that the terms depending only on t, namely

$$\frac{1}{\cosh^2 t}, \quad \frac{\sinh t}{\cosh^3 t}, \quad \text{and} \quad \frac{\sinh^2 t}{\cosh^4 t},$$

are smooth and bounded on the compact interval $[t_1, t_2]$, since the hyperbolic sine and cosine functions are continuous and differentiable everywhere, and $[t_1, t_2]$ is a finite closed interval. Therefore, since $|v(t)+\varphi(t)| \leq \|\varphi\|_\infty + \|v\|_\infty \leq \|\varphi\|_\infty + M$, there exist constants C_1, C_2 such that

$$|f(v(t)+\varphi(t),t)| \leq C_1 + C_2|v(t)+\varphi(t)| \leq C_1 + C_2 M =: L_H.$$

Then for all $v \in K$,

$$|Tv(t)| \leq \|\varphi\|_\infty + \int_{t_1}^{t_2} G(t,s)|f(v(s)+\varphi(s),s)|ds \leq \|\varphi\|_\infty + L_H \cdot \max_{t\in[t_1,t_2]}\int_{t_1}^{t_2} G(t,s)\,ds.$$

Integration of $G(t,s)$ on $[t_1, t_2]$ yields:

$$\int_{t_1}^{t_2} G(t,s)\,ds = \frac{(t_2-t)(t-t_1)}{2}.$$

This function attains its maximum when $t = \frac{t_1+t_2}{2}$, leading to

$$\max_{t\in[t_1,t_2]}\int_{t_1}^{t_2} G(t,s)\,ds = \frac{(t_2-t_1)^2}{8}.$$

Therefore,

$$\|Tv\|_\infty \leq \|\varphi\|_\infty + L_H \cdot \frac{(t_2-t_1)^2}{8}.$$

Choose

$$M := \|\varphi\|_\infty + L_H \cdot \frac{(t_2-t_1)^2}{8}$$

so that $T(K) \subseteq K$.

Since f is continuous, the operator T is continuous as well. The image $T(K)$ is equicontinuous and uniformly bounded because $G(t,s)$ is smooth and $f(u,t)$ is bounded on bounded sets. By the Arzelà–Ascoli Theorem [20], T is compact. Since $T : K \to K$ is continuous and compact, and maps the closed convex set K into itself, Schauder's Fixed Point Theorem [19] guarantees the existence of a fixed point $v \in K$ such that $Tv = v$. This function $v \in C^2([t_1, t_2])$ solves the equation (3.7) with boundary conditions $v(t_1) = v(t_2) = 0$. Since $\varphi(t)$ is smooth and uniquely determined by the boundary values (2.14), the function $u = v + \varphi \in C^2([t_1, t_2])$ solves the original problem (2.12) with boundary conditions (2.14).

3.3. Uniqueness of solution

Having established existence, now the uniqueness of the found solution needs to be proven. This follows from the theorem below.

Theorem 3.2

Assume that the conditions of Theorem 3.1 hold. Let $F \in C(\mathbb{R})$, $\rho \in C^1(\mathbb{R})$ in equation (2.12), and assume the following conditions hold:

- *F is Lipschitz continuous:*

$$|F(u_1) - F(u_2)| \leq N_F|u_1 - u_2|; \tag{3.13}$$

- *ρ is bounded below:*

$$\rho(u) \geq \rho_{\min} > 0 \quad \text{for all} \quad u \in \mathbb{R}; \tag{3.14}$$

- ρ' is Lipschitz continuous:

$$|\rho'(u_1) - \rho'(u_2)| \le N_{\rho'}|u_1 - u_2|; \tag{3.15}$$

-

$$\left|\frac{\rho'(u)}{\sqrt{\rho(u)}}\right| \le 2m \quad \text{for some constant} \quad m > 0, \tag{3.16}$$

which implies that $\sqrt{\rho(u)}$ is Lipschitz continuous with constant $N_{\sqrt{\rho}} := m$

Then differential equation (2.12) with boundary conditions (2.14) has an unique solution on $[t_1, t_2]$ with

$$N := \sup_{t \in [t_1, t_2]} \left(\frac{1}{\cosh^2 t}\left(N_F + \omega \cdot \frac{N_{\sqrt{\rho}}}{\sqrt{\rho_{\min}}} + \frac{\omega^2 N_{\rho'}}{2}\right)\right) < \frac{8}{(t_2 - t_1)^2}.$$

Proof

Let $u_1(t)$ and $u_2(t)$ be two classical solutions with the same boundary conditions $u(t_1) = \alpha_1$ and $u(t_2) = \alpha_2$. Define $u_j(t) = v_j(t) + \varphi(t)$ for $j = 1, 2$, where $\varphi(t)$ is the same as in (3.6), satisfying (3.5). Then v_i satisfies boundary conditions $v(t_1) = v(t_2) = 0$ and

$$v_j(t) = \int_{t_1}^{t_2} G(t, s) f(v_j(s) + \varphi(s), s)\, ds,$$

where $f(u(t), t)$ is the nonlinearity in (3.2) and $G(t, s)$ is the Green's function for the Dirichlet Laplacian on $[t_1, t_2]$ in (3.3).

Define $w(t) := v_1(t) - v_2(t)$. Then

$$w(t) = \int_{t_1}^{t_2} G(t, s) \left[f(u_1(s), s) - f(u_2(s), s)\right] ds,$$

where $u_i(s) = v_i(s) + \varphi(s)$. Taking the supremum norm yields

$$\|w\|_\infty \le \sup_{t \in [t_1, t_2]} \int_{t_1}^{t_2} G(t, s) |f(u_1(s), s) - f(u_2(s), s)|\, ds.$$

Now the Lipschitz constant of each term in the function $f(u, t)$ is estimated. Let us recall $f(u, t)$ for convenience:

$$f(u(t), t) = \frac{F(u)}{\cosh^2 t} - 2\omega \frac{\sinh t}{\cosh^3 t}\sqrt{\rho(u)} - \frac{\omega^2 \rho'(u)\sinh^2 t}{2\cosh^4 t}.$$

The first term $F(u)/\cosh^2 t$ is Lipschitz in u with constant $N_F/\cosh^2 t$, where N_F is a Lipschitz constant for F.

For the second term, write

$$\left|\frac{\sinh t}{\cosh^3 t}\sqrt{\rho(u)}\right| \le \frac{|\sinh t|}{\cosh^3 t}\sqrt{\rho(u)}.$$

Differentiating with respect to u, and using the chain rule, the Lipschitz contribution is bounded by

$$\omega \cdot \frac{N_{\sqrt{\rho}}}{\sqrt{\rho_{\min}}} \cdot \frac{|\sinh t|}{\cosh^3 t}.$$

Since $|\sinh t| \le \cosh t$, we have

$$\frac{|\sinh t|}{\cosh^3 t} \le \frac{1}{\cosh^2 t}.$$

Hence, the second term is Lipschitz in u with constant bounded by

$$\omega \cdot \frac{N_{\sqrt{\rho}}}{\sqrt{\rho_{\min}}} \cdot \frac{1}{\cosh^2 t}.$$

For the third term, the Lipschitz constant of ρ' is $N_{\rho'}$, and the bound

$$\frac{\sinh^2 t}{\cosh^4 t} \le \frac{1}{\cosh^2 t},$$

is obtained so the Lipschitz constant of the third term is bounded by

$$\frac{\omega^2 N_{\rho'}}{2} \cdot \frac{1}{\cosh^2 t}.$$

Thus,

$$|f(u_1(t), t) - f(u_2(t), t)| \leq \tilde{N}(t) \cdot |w(t)|,$$

where

$$\tilde{N}(t) := \frac{1}{\cosh^2 t} \left(N_F + \omega \cdot \frac{N_{\sqrt{\rho}}}{\sqrt{\rho_{\min}}} + \frac{\omega^2 N_{\rho'}}{2} \right)$$

Define $N := \sup_{t \in [t_1, t_2]} \tilde{N}(t)$, so that

$$|f(u_1(t), t) - f(u_2(t), t)| \leq N \cdot |w(t)|.$$

This yields

$$\|w\|_\infty \leq N \cdot \sup_{t \in [t_1, t_2]} \int_{t_1}^{t_2} G(t, s) \, ds \cdot \|w\|_\infty.$$

From the existence proof, it is known that

$$\sup_{t \in [t_1, t_2]} \int_{t_1}^{t_2} G(t, s) \, ds = \frac{(t_2 - t_1)^2}{8}.$$

Hence,

$$\|w\|_\infty \leq \|w\|_\infty \cdot N \cdot \frac{(t_2 - t_1)^2}{8}.$$

If $N < \frac{8}{(t_2 - t_1)^2}$, the only possibility is $\|w\|_\infty = 0$, and thus $w(t) = 0$ for all t. This implies $u_1(t) = u_2(t)$, and uniqueness is proven.

4

Numerical Analysis

In this chapter, the behaviour of ACC is investigated through numerical simulations of the model (2.12). The primary goal is to understand how different choices of forcing and density stratification influence the structure and stability of the stream function $u(t)$.

Let us recall the model that will be numerically analysed in this chapter:

$$u''(t) = \frac{F(u(t))}{\cosh^2 t} - 2\omega \frac{\sinh t}{\cosh^3 t} \sqrt{\rho(u(t))} - \frac{\omega^2 \rho'(u(t)) \sinh^2 t}{2\cosh^4 t}, \qquad t \in [t_1, t_2], \tag{4.1}$$

with boundary conditions

$$u(t_1) = u(t_2) = 0. \tag{4.2}$$

The chapter is structured as follows. The first part presents a numerical solution for a linear vorticity function and linear stratification. Then, the numerical solution is compared to an exact analytic solution in the simplified case where both F and ρ are constant. After that, different functions of $\rho(u)$ are explored for our model.

4.1. Numerical solution

In this section, a numerical solution to (4.1) is computed. The model is solved numerically with a fixed choice of domain, boundary conditions, and parameters. The numerical method is implemented, after which the chosen functions are verified to satisfy the assumptions required for existence and uniqueness, and the resulting solution is analysed. Finally, the stability of the solution is discussed.

4.1.1. Numerical Setup

Consider the BVP on the interval $t \in [0, 1]$. This domain represents a finite latitudinal band around Antarctica. The radial coordinate t is dimensionless, and the model is non-dimensionalised such that physical length scales are encoded in the parameters, rather than in the domain itself. Choosing the interval $[0, 1]$ simplifies the numerical implementation. After this domain choice, homogeneous Dirichlet boundary conditions (2.13) are imposed. This corresponds to a stream function that vanishes at both the inner and outer bounds of the ACC.

The rotation parameter ω, which represents the Coriolis forcing, is defined as $\omega = \frac{\Omega R}{c}$, where $\Omega = 7.292115 \times 10^{-5}$ rad/s is the angular velocity of the Earth, $R = 6.371137 \times 10^6$ m is the Earth's mean radius [17], and $c = 0.1$ m/s is a representative velocity scale for large-scale ocean currents [16]. Substituting these values gives $\omega \approx 4650$, which is used throughout the numerical analysis.

The vorticity function is chosen as $F(u) = -u$, which models a linear restoring force [15]. This form is mathematically convenient and represents internal forcing in large-scale geophysical flows. The density function is taken to be $\rho(u) = 1 + \beta u$, with $\beta = 0.005$, representing a weak linear stratification. This simple form couples the stream function with the density variation without introducing strong non-linearity. These function are simple yet physically interpretable.

4.1.2. Validation of Assumptions and Numerical Implementation

Before computing the numerical solution, it is first verified that the chosen model setup satisfies the assumptions required for the existence and uniqueness of a solution. In particular, Theorem 3.1 guarantees existence of a classical solution under continuity and boundedness assumptions on the vorticity and density functions, and Theorem 3.2 establishes uniqueness under additional Lipschitz conditions.

First, the assumptions on the vorticity function $F(u) = -u$ are examined. This function is globally continuous and differentiable on $\mathbb{R}$, with derivative $F'(u) = -1$. Since the derivative is bounded and F is linear , it is Lipschitz continuous on $\mathbb{R}$ with Lipschitz constant $N_F = 1$. And, this constant also satisfies the condition required for uniqueness:

$$N < \frac{8}{(t_2 - t_1)^2}, \quad \text{with } N = 1 \text{ and } t_2 - t_1 = 1,$$

where $t_2 - t_1 = 1$, yielding $N = 1 < 8$. The vorticity function also satisfies the linear growth condition

$$|F(u)| \leq L_F(1 + |u|), \quad \text{with } L_F = 1.$$

Next, the assumptions on the density function $\rho(u) = 1 + \beta u$, with $\beta = 0.005$, are checked. This function is continuously differentiable on $\mathbb{R}$, with

$$\rho'(u) = \beta.$$

The derivative is constant and therefore bounded by β. After substituting $\beta = 0.005$ into $\rho(u) = 1 + \beta u$ and rewriting, it follows that $\rho(u)$ is strictly positive if $u > -1/\beta = -200$. This condition will be numerically verified after plotting our BVP (4.1)-(4.2). For uniqueness, it is required that ρ' is Lipschitz continuous, which holds trivially since $\rho'(u) = \beta$ is constant. Furthermore, the function $\sqrt{\rho(u)}$ must be Lipschitz continuous. This follows from the boundedness of

$$\left| \frac{\rho'(u)}{\sqrt{\rho(u)}} \right| = \frac{\beta}{\sqrt{1 + \beta u}},$$

which is maximal when u is minimal. To ensure this expression is bounded, the safety condition $u(t) > -199.9$ is imposed, which guarantees

$$\left| \frac{\rho'(u)}{\sqrt{\rho(u)}} \right| \leq \frac{0.005}{\sqrt{1 + 0.005 \cdot (-199.9)}} = \frac{0.005}{\sqrt{0.0005}} \approx 0.2236.$$

In summary, all assumptions (3.10)-(3.16) of Theorems 3.1 and 3.2 are theoretically satisfied under the condition that the numerical solution satisfies $u(t) > -199.9$ for all $t \in [0, 1]$.

To verify this, the BVP (4.1)-(4.2) was solved using the collocation method implemented in `scipy.integrate.solve_bv`. The second-order differential equation (4.1) was reformulated as a first-order system:

$$\begin{cases} y_1' = y_2, \\ y_2' = -\dfrac{y_1}{\cosh^2 t} - \dfrac{2\omega \sinh t}{\cosh^3 t} \sqrt{1 + \beta y_1} - \dfrac{\omega^2 \beta \sinh^2 t}{2 \cosh^4 t}, \end{cases} \quad \text{with } y_1(0) = y_1(1) = 0,$$

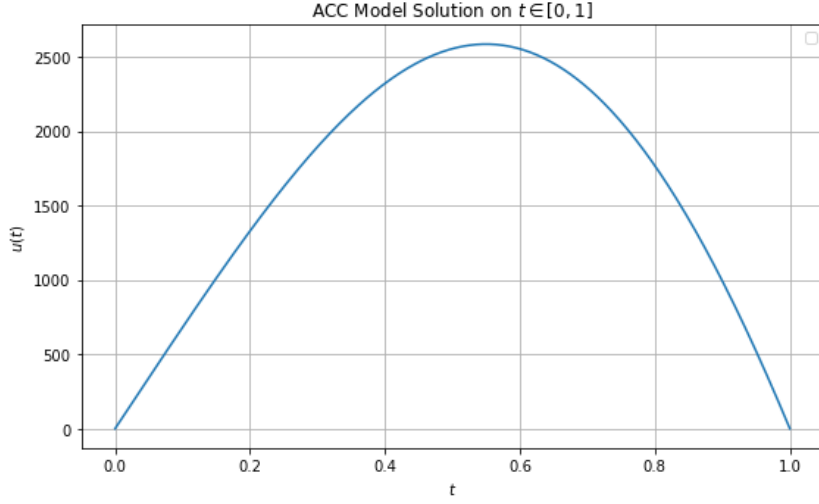where $y_1(t) = u(t)$ and $y_2(t) = u'(t)$. The solution is shown in Figure 4.1

Figure 4.1: Numerical solution of BVP (4.1)-(4.2) with $F(u) = -u$, $\rho(u) = 1 + 0.005u$.

The numerical solution in Figure 4.1 confirms that $u(t)$ remains above -199.9 throughout the domain. Therefore, all theoretical assumptions (3.10)-(3.16) are indeed validated.

To further illustrate that $F(u)$ and $\rho(u)$ behave smoothly and satisfy the required assumptions, these functions are also plotted in Figure 4.2, evaluated along the computed solution $u(t)$. This confirms that the assumptions are not only satisfied numerically, but also behave as expected across the domain.
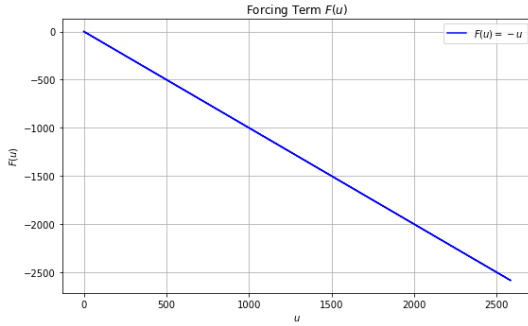
(a) Forcing function $F(u(t)) = -u(t)$. The function is linear, continuous, and satisfies the Lipschitz condition with constant $N_F = 1$.
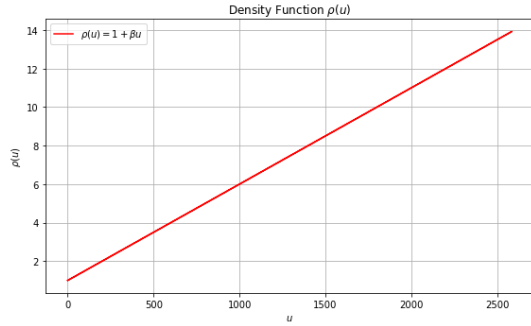
(b) Density function $\rho(u(t)) = 1 + \beta u(t)$ with $\beta = 0.005$. The function is strictly positive and continuously differentiable with constant derivative $\rho'(u) = \beta$.

Figure 4.2: Plots of the vorticity forcing term $F(u)$ and the density function $\rho(u)$ evaluated along the numerical solution $u(t)$.

The shape of the solution in Figure 4.1 means that the flow is strongest in the middle part of the domain and weak near the edges. The central peak suggests a jet-like structure in the domain, which is physically consistent with observations of the ACC [12]. The maximum is attained at $t = 0.549098$, which shows that the solution is nearly symmetric around the midpoint of the domain.

The density function $\rho(u) = 1 + \beta u$ mildly modulates the baroclinic response. Since u varies moderately and β is small, the gradient remains weak. Stronger non-linearities such as tanh or exponential forms could lead to asymmetry or multiple peaks. This effect is examined further in later sections.

4.1.3. Stability of the Solution

An important requirement for any non-linear BVP is the stability of its solutions under small perturbations in the input data. In our model, this means that small variations in the boundary conditions or parameters should not lead to disproportionately large deviations in the numerical solution.

The uniqueness theorem already provides a theoretical basis for proving such stability. Under the assumptions (3.13)-(3.16), the solution depends continuously on the boundary data. In particular, the Lipschitz continuity of $F(u)$ ensures that small perturbations in the input data yield proportionally small derivations

in the solution.

To verify this numerically, a boundary perturbation test is conducted. The problem is solved twice: once with the original boundary conditions (2.13), and once with a small perturbation to the right boundary, replacing $u(1) = 0$ with $u(1) = 0.01$. The solutions are compared pointwise over the interval $[0, 1]$. The deviation between the solutions remained uniformly small across the domain, with a maximum deviation of approximately 0.0103, as shown in Figure 4.3. This is of the same order as the magnitude of the perturbation, which confirms that the solution is numerically stable.
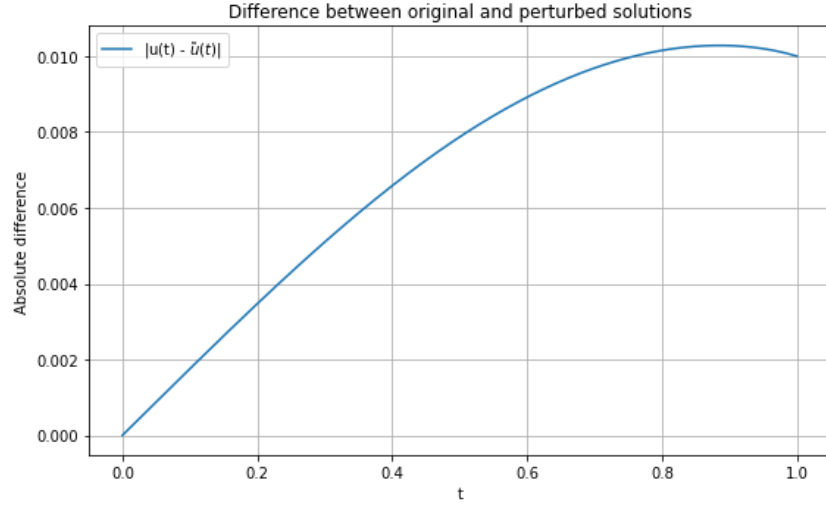

Figure 4.3: Pointwise difference between original and perturbed solution ($u(1) = 0.01$), confirming boundary stability.

The Python code used for this test is provided in Appendix A2.1.

In addition to the boundary perturbation test, a linearised stability test is performed. This method is based on linearising the non-linear BVP around the previously computed solution $u(t)$. Specifically, a perturbed solution of the form $u(t) + \delta u(t)$ is considered, where $\delta u(t)$ is a small perturbation. Substituting this expression into the original equation (4.1) the following second-order linearised equation is obtained:

$$\delta u''(t) = \frac{\partial f}{\partial u}(u(t), t) \cdot \delta u(t),$$

where $f(u, t)$ is the right-hand side of (4.1) just as before.

The linearised system is solved numerically using the same collocation method as before, with homogeneous Dirichlet boundary conditions for δu, and is plotted in Figure 4.4.
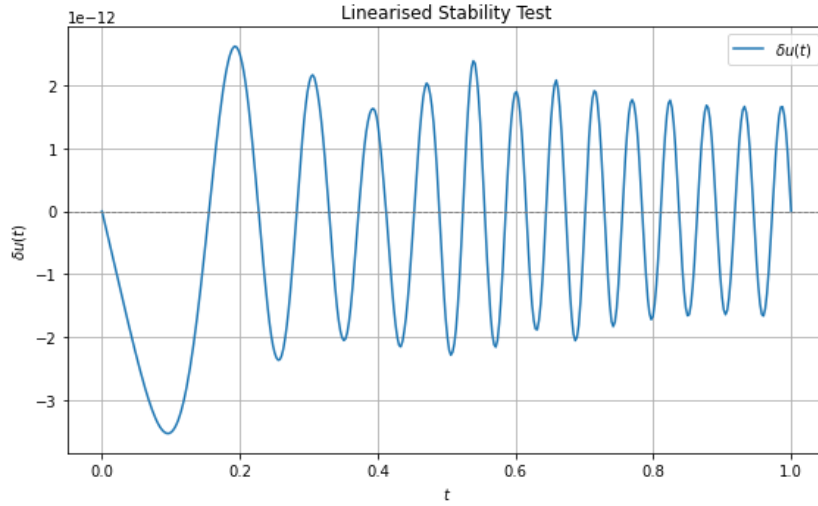
Figure 4.4: Linearised stability test showing bounded variation $\delta u(t)$.

As shown in Figure 4.4, the perturbation $\delta u(t)$ remains small across the entire domain, and does not exhibit exponential growth or instability. This proves that the computed solution is not only stable with respect to its boundary conditions, but also internally robust to small variations.

The Python code used for this test is provided in Appendix A2.2.

4.2. Comparison with Analytic Solution for Constant Forcing and Density

To validate the numerical method and confirm the stability and reliability of our model, an analytic solution in the special case where both the vorticity forcing and the density are constant is derived. Specifically, take

$$F(u) = 100, \qquad \rho(u) = 1,$$

which simplifies the original non-linear differential equation (4.1) to an equation that depends only on t:

$$u''(t) = \frac{100}{\cosh^2(t)} - 2\omega \cdot \frac{\sinh(t)}{\cosh^3(t)}. \tag{4.3}$$

Equation (4.3) can be solved by direct integration. The first integration yields

$$u'(t) = 100 \tanh(t) + \omega \cdot \frac{1}{\cosh^2(t)} + A, \tag{4.4}$$

where A is an integration constant. The second integration then gives the general solution

$$u(t) = 100 \log(\cosh(t)) + \omega \tanh(t) + At + B, \tag{4.5}$$

where B is a second integration constant. The constants A and B are determined by applying the boundary conditions $u(0) = u(1) = 0$. Solving the resulting system yields the unique solution satisfying the boundary conditions. It is given by

$$u(t) = 100 \left(\log(\cosh(t)) - t \log(\cosh(1)) \right) + \omega \left(\tanh(t) - t \tanh(1) \right). \tag{4.6}$$

This function satisfies both boundary conditions and is smooth on $[0, 1]$. The exact solution (4.6) is used to evaluate the accuracy of the numerical solver by comparing this expression to the numerical solution obtained with `scipy.integrate.solve_bvp`. Figure 4.5 shows the comparison between the analytic and the numerical solution.
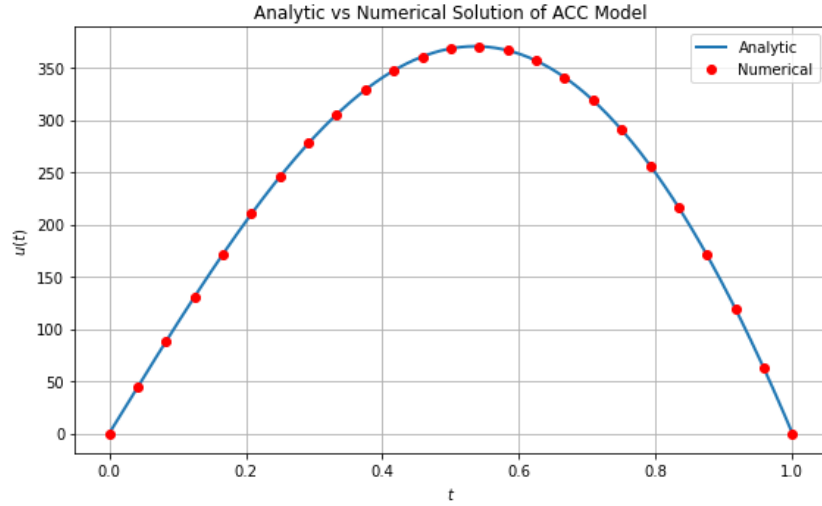
Figure 4.5: Comparison between analytic and numerical solutions for $F(u) = 100$ and $\rho(u) = 1$.

The numerical solution is evaluated at 25 evenly spaced points, while the analytic function is plotted as a continuous line. To quantify the agreement, both solutions at $t = 0.5$ are compared:

$$u_{\text{numerical}}(0.5) = 368.46077715, \quad u_{\text{analytic}}(0.5) = 368.46077783,$$

with an absolute error less than 10^{-6}. This confirms the numerical solver achieves high accuracy and correctly captures the structure of the solution in this simplified case. This does not guarantee that the method will remain accurate in settings where F and ρ are not constant. However, it strongly suggests that the collocation solver performs reliably when applied under similar model assumptions.

4.3. Testing Different Stratification Profiles $\rho(u)$

To better understand how stratification affects the solution of the ACC model, the behaviour of the system under different choices of the function $\rho(u)$ is studied. First, the vorticity function is fixed to the linear case $F(u) = -u$, and five different functions for $\rho(u)$ are tested. These represent simplified but physically plausible models of how the density might depend on the stream function. The following five functions are considered:

- Constant: $\rho(u) = 1$
- Linear: $\rho(u) = 1 + \beta u$
- Quadratic: $\rho(u) = 1 + \beta u^2$
- Saturating: $\rho(u) = 1 + \tanh(\beta u)$
- Exponential: $\rho(u) = \exp(\beta u)$

These choices capture a range of behaviours, from no stratification to moderate, strong and saturating stratification. In all cases, the parameter $\beta = 0.005$ is used, consistent with earlier sections. The numerical solutions are obtained using the collocation method again and plotted together in Figure 4.6.
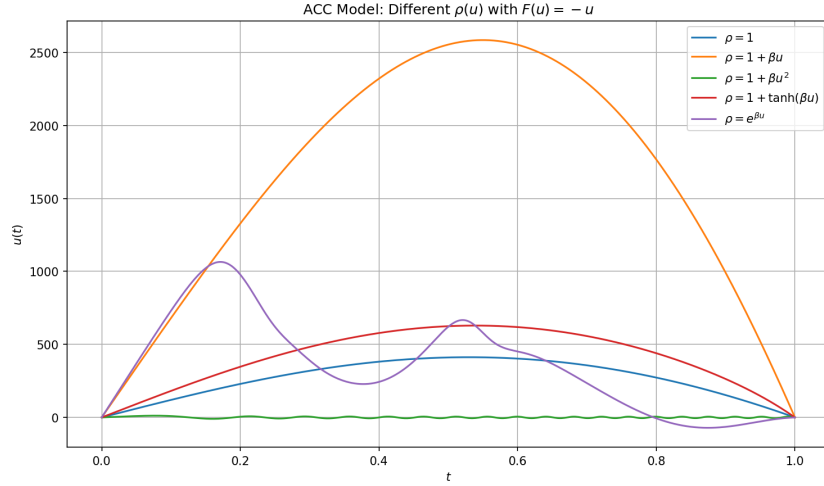
Figure 4.6: Numerical solutions of the ACC model with fixed $F(u) = -u$ and five different density functions $\rho(u)$.

The results demonstrate that the choice of function $\rho(u)$ has a strong influence on the shape, amplitude, and symmetry of the solution $u(t)$. The constant case ($\rho(u) = 1$) gives a baseline reference and yields a smooth, almost symmetric solution. When the density increases linearly with u, as in $\rho(u) = 1 + \beta u$, the solution has a much higher amplitude. This reflects a stronger non-linear response of the system to variations in the flow.

The saturating profile $\rho(u) = 1 + \tanh(\beta u)$ leads to a solution that is similar to the linear and constant case in shape. The amplitude is higher than in the constant case but avoids the the non-linear escalation seen in the quadratic and exponential cases. This is consistent with the saturating effect of the hyperbolic tangent function, which limits the growth of $\rho(u)$ for large u.

In contrast, the quadratic profile leads to a very different solution. The resulting curve shows oscillations whose frequency increases across the domain, as can be seen more clearly in a zoomed-in view of the solution in Figure 4.7.
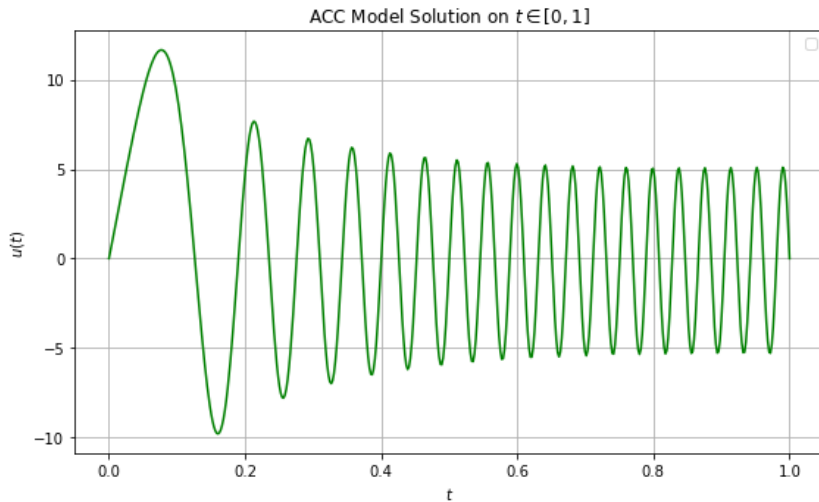

Figure 4.7: Zoomed-in view of the numerical solution for $\rho(u) = 1 + \beta u^2$ and $F(u) = -u$.

These oscillations come from the strong non-linear terms introduced by both the u^2 term and its derivative. Since $\rho'(u) = 2\beta u$, even moderate values of u can cause steep changes in the coefficients of the equation. This leads to rapid local variations that are numerically challenging and physically less interpretable. Although the solution remains bounded, its oscillatory nature suggests reduced stability and makes this profile less suited for geophysical flow applications.

The exponential profile, while mathematically well-defined, results in a numerically unstable solution.

Although a curve is plotted in Figure 4.6, the solution fails internal convergence criteria of the solver and shows unphysical oscillations and rapid growth. Multiple attempts were made, including lowering the initial guess amplitude, reducing the parameter β, and increasing the solver tolerance and mesh refinement. None of these adjustments gave a reliable or convergent solution. These problems arise from the numerical stiffness caused by the rapid increase of $\exp(\beta u)$ for even moderate u, which makes the model hard to solve accurately. In addition, note that once $u(t)$ grows too large, the assumptions that $\rho(u)$ and $\rho'(u)$ remain bounded are no longer satisfied. As a result, the exponential case not only suffers from numerical instability but also fails the theoretical assumptions that guarantee existence and uniqueness of the solution.

In conclusion, all functions $\rho(u)$ except the exponential case satisfy the assumptions of the existence and uniqueness theorems discussed earlier. However, the exponential case pushes the limits of numerical stability and highlights the importance of choosing $\rho(u)$ carefully in both modelling and computation. This analysis confirms that the model responds sensitively to different stratification functions, and that even small changes in the form of $\rho(u)$ can lead to very different solution behaviours. In applied settings, choosing an appropriate stratification function should be guided by physical reasoning and supported by numerical testing as shown here.

To explore whether the influence of stratification depends on the choice of vorticity forcing, the analysis is repeated with different choices for the forcing term $F(u)$. In particular, two different functions are tested that fully satisfy the theoretical assumptions: a sinusoidal forcing $F(u) = -\sin(u)$, which is smooth and globally Lipschitz continuous, and a constant forcing $F(u) = 100$, which removes all dependence on u. Figure 4.8 shows the results for these two cases, using the same density functions $\rho(u)$ as before.

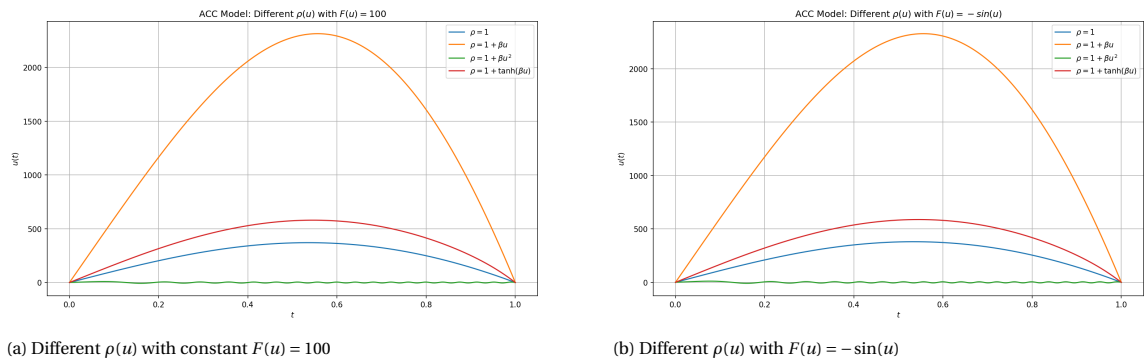(a) Different $\rho(u)$ with constant $F(u) = 100$ (b) Different $\rho(u)$ with $F(u) = -\sin(u)$

Figure 4.8: Comparison of model solutions $u(t)$ for different density functions $\rho(u)$, using (a) $F(u) = 100$ and (b) $F(u) = -\sin(u)$.

The solution curves are very similar to those obtained with the original linear forcing $F(u) = -u$. The constant and linear density profiles again produce smooth and almost symmetric solutions with moderate to large amplitude. The saturating case $\rho(u) = 1 + \tanh(\beta u)$ lies between the constant and linear profiles and shows stable behaviour. The quadratic profile leads to oscillations across the domain, consistent with earlier observations. The exponential density function $\rho(u) = \exp(\beta u)$ is again left out, as it remains numerically unstable across the two forcing functions tested.

To explore how the model behaves when the assumptions for existence and uniqueness of the solution are not satisfied, also tested two more cases are tested: an exponential forcing $F(u) = \exp(\beta u)$, which is not globally Lipschitz continuous, and a cubic forcing $F(u) = -u^3$, which is smooth but grows too rapidly for the theoretical results to apply. These two cases are both plotted in Figure 4.9.
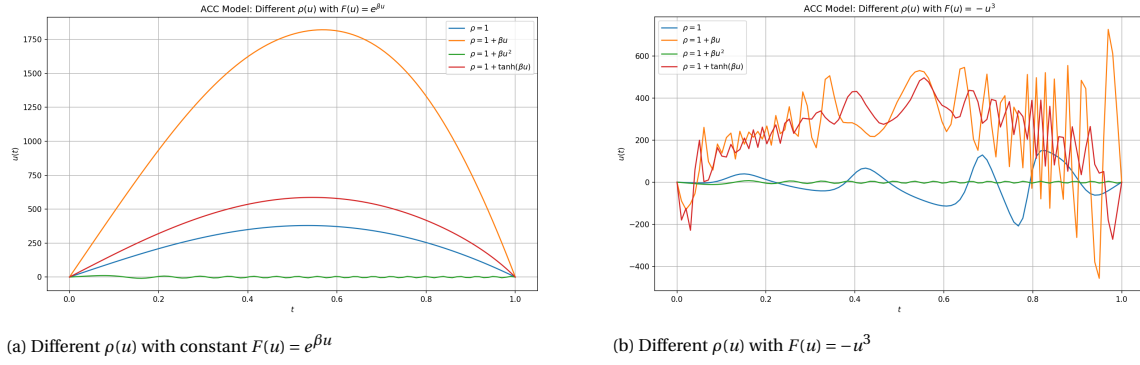
(a) Different $\rho(u)$ with constant $F(u) = e^{\beta u}$ (b) Different $\rho(u)$ with $F(u) = -u^3$

Figure 4.9: Comparison of model solutions $u(t)$ for different density functions $\rho(u)$, using (a) $F(u) = e^{\beta u}$ and (b) $F(u) = -u^3$.

Surprisingly, the exponential forcing produced well-behaved numerical solutions for all density profiles except, of course, the exponential density profile. While the assumptions are technically violated, the solver converged and returned stable results. This suggests that the method can tolerate some mild deviations from the theoretical framework, although such cases must be interpreted with caution.

In contrast, the cubic forcing term led to severe numerical instability. The solver failed to converge in most cases, especially when finer grids were used. The output showed signs of unbounded growth and erratic oscillations (see Figure 4.9b), and in some runs, numerical errors were triggered due to negative arguments in the square root of $\rho(u)$. This breakdown illustrates how strongly non-linear forcing functions can destabilise the model, even when $\rho(u)$ itself is well behaved.

In summary, the model appears robust under moderate changes to the forcing function, provided that the theoretical assumptions remain approximately satisfied. When the assumptions are clearly violated, such as in the cubic case, stability is no longer guaranteed, and numerically unstable behaviour may emerge.

5

Conclusion and Discussion

This chapter reflects on the main findings of the analytical and numerical study presented in the previous chapters. The broader implications of the model are discussed, its strengths and limitations are critically evaluated, and potential directions for future research are outlined.

5.1. Conclusion

This report analysed a simplified mathematical model for the ACC, focusing on the influence of density stratification on the steady-state flow. The model formulation led to a non-linear BVP for the stream function $u(t)$, incorporating a prescribed forcing $F(u)$ and density function $\rho(u)$. Under reasonable assumptions, the model was shown to be mathematically well-posed: a solution exists and is unique when $F(u)$ and $\rho(u)$ satisfy smoothness and boundedness conditions. These results provide a solid theoretical foundation for interpreting solutions to the model as physically meaningful.

Numerical implementation of the model using a collocation method yielded a stream function profile with a pronounced central jet. Validation against an analytic solution in a simplified case confirmed the accuracy of the numerical solver, and additional stability tests showed that small perturbations to boundary conditions or model inputs led to only minor changes in the outcome. This confirms both the reliability of the numerical method and the robustness of the solution.

A key outcome of this report is the identification of strong sensitivity in the ACC stream function to the choice of the density function $\rho(u)$. While moderate stratification profiles resulted in stable and interpretable solutions, strongly non-linear or rapidly growing profiles could lead to oscillations and numerical instability. Similar findings held for the forcing function: standard forms such as $F(u) = -u$ or $F(u) = \sin(u)$ behaved well, but more extreme nonlinearity in $F(u)$ could destabilise the solution.

Overall, this report has shown that a simplified one-dimensional model can capture key qualitative features of ACC dynamics while remaining mathematically tractable. It combines analytic proofs with numerical analysis to investigate how different physical assumptions affect the structure of the solution. The results offer insight into the mechanisms that shape ocean flows and lay the groundwork for future model extensions that can include more realistic oceanographic conditions.

5.2. Limitations

While the simplified ACC model provides useful analytical and numerical insights, it is important to recognise its limitations. By construction, the model is axisymmetric and time-independent, focusing on a steady-state stream function that varies only with a radial coordinate t. This means transient dynamics and longitudinal variations (such as localised eddies or the effect of continents and topography) are neglected. In reality, the ACC has multiple fronts and significant longitudinal variability due to land-ocean geometry and time-dependent eddies [13]. The model assumes a fixed domain bounded by latitudes, treating the ACC as a concentric flow around Antarctica. This is an abstraction; for example, the northern boundary of the actual ACC is not a perfect circle and is influenced by continents, with constrictions such as the Drake Passage [13].

Additionally, the model uses a single-layer shallow-water approximation [4] with a prescribed stratification profile $\rho(u)$. In reality, the ACC's stratification arises from a multi-layer fluid with continuous density

variation in depth and has complex dynamics such as vertical shear and baroclinic instabilities [13]. These are beyond the scope of the one-dimensional model.

Moreover, the forcing function $F(u)$ represents the vorticity input due to external forces, primarily wind stress [3]. In the model, $F(u)$ was often taken to be linear or constant for mathematical convenience, whereas real wind stress profiles vary with latitude and can induce multiple jets. This idealisation therefore limits the model's ability to capture the full dynamical impact of realistic wind forcing.

5.3. Recommendations for Further Research

Several directions can be pursued to extend the model and address its limitations. One natural extension is to introduce time dependence to investigate the stability of the ACC solution and the possible development of eddies or waves. By extending the model to an unsteady evolution equation, for example a time-dependent shallow water system or a time-dependent solver for the BVP, it could studied whether the steady solution found is dynamically stable or prone to oscillations over time [15].

Another extension is to incorporate multiple vertical layers or a continuous stratification in a more explicit way. Instead of a single $\rho(u)$ relationship, a multi-layer shallow-water model could capture baroclinic modes and give insight into how density variations with depth influence the surface flow [1].

It would also be interesting to add realistic wind-forcing profiles. For instance, a latitude-dependent F that peaks where westerly winds are strongest and see if the model then produces multiple stream function peaks resembling the observed fronts of the ACC.

In summary, the model demonstrates an insightful mathematical model of the ACC's flow with density variations. There remain many ways to improve and build upon this foundation. Future work can make the model more realistic and comprehensive, while retaining the analytical tractability that makes it a useful tool for understanding the fundamental dynamics of the world's strongest current.
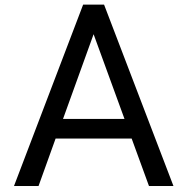
Python Codes for Numerical Analysis

A.1. Python Code for Numerical solution

```python
import numpy as np
import matplotlib.pyplot as plt
from scipy.integrate import solve_bvp

omega = 4650
beta = 0.005

def F(u):
    return -u

def rho(u):
    return 1 + beta * u

def rho_prime(u):
    return beta * np.ones_like(u)

def acc_model(t, y):
    u = y[0]
    up = y[1]
    cosh_t = np.cosh(t)
    sinh_t = np.sinh(t)
    rho_val = rho(u)
    drho_val = rho_prime(u)
    F_val = F(u)
    u_double_prime = (
        F_val / cosh_t**2
        - 2 * omega * np.sqrt(rho_val) * sinh_t / cosh_t**3
        - omega**2 * drho_val * sinh_t**2 / (2 * cosh_t**4)
    )
    return np.vstack((up, u_double_prime))

# Boundary conditions: u(t1) = 0, u(t2) = 0
def bc(ya, yb):
    return np.array([ya[0], yb[0]])


t1, t2 = 0, 1
t_init = np.linspace(t1, t2, 100)
```

```python
u_guess = 0.1 * np.sin(np.pi * (t_init - t1) / (t2 - t1))
du_guess = 0.1 * (np.pi / (t2 - t1)) * np.cos(np.pi * (t_init - t1) / (t2 - t1))
y_guess = np.vstack((u_guess, du_guess))


solution = solve_bvp(acc_model, bc, t_init, y_guess)
print("Success:", solution.success)

t_fine = np.linspace(t1, t2, 500)
u_fine = solution.sol(t_fine)[0]

u_max = np.max(u_fine)
t_at_umax = t_fine[np.argmax(u_fine)]
print(f"Maximum u(t): {u_max:.6f} at t = {t_at_umax:.6f}")


plt.figure(figsize=(8, 5))
plt.plot(t_fine, u_fine)
plt.title('ACC Model Solution on $t \in [0, 1]$')
plt.xlabel(r'$t$')
plt.ylabel(r'$u(t)$')
plt.grid(True)
plt.legend()
plt.tight_layout()
plt.show()

# Plot rho(u(t))
# plt.figure(figsize=(8, 5))
# plt.plot(u_fine, rho_vals, label=r'$\rho(u) = 1 + \beta u$', color='red')
# plt.title(r'Density Function $\rho(u)$')
# plt.xlabel(r'$u$')
# plt.ylabel(r'$\rho(u)$')
# plt.grid(True)
# plt.legend()
# plt.tight_layout()
# plt.show()


# # Plot F(u(t))
# plt.figure(figsize=(8, 5))
# plt.plot(u_fine, F_vals, label=r'$F(u) = -u$', color='blue')
# plt.title('Forcing Term $F(u)$')
# plt.xlabel(r'$u$')
# plt.ylabel(r'$F(u)$')
# plt.grid(True)
# plt.legend()
# plt.tight_layout()
# plt.show()
```

A.2. Added Python Code for Numerical Stability

A.2.1. First method

```python
def bc(ya, yb):
    return np.array([ya[0], yb[0]])


def bc_perturbed(ya, yb):
```

```
        return np.array([ya[0], yb[0] - 0.01])


t1, t2 = 0, 1
t_init = np.linspace(t1, t2, 100)
u_guess = 0.1 * np.sin(np.pi * (t_init - t1) / (t2 - t1))
du_guess = 0.1 * (np.pi / (t2 - t1)) * np.cos(np.pi * (t_init - t1) / (t2 - t1))
y_guess = np.vstack((u_guess, du_guess))


sol_orig = solve_bvp(acc_model, bc, t_init, y_guess)
sol_pert = solve_bvp(acc_model, bc_perturbed, t_init, y_guess)


t_fine = np.linspace(t1, t2, 500)
u_orig = sol_orig.sol(t_fine)[0]
u_pert = sol_pert.sol(t_fine)[0]
diff = np.abs(u_orig - u_pert)


plt.figure(figsize=(8, 5))
plt.plot(t_fine, diff, label="|u(t) - $\˜u(t)$|")
plt.title("Difference between original and perturbed solutions")
plt.xlabel("t")
plt.ylabel("Absolute difference")
plt.grid(True)
plt.legend()
plt.tight_layout()
plt.show()

max_diff = np.max(diff)
print("Maximum deviation:", max_diff)
```

A.2.2. Second method

```
def F_prime(u): return -np.ones_like(u)

# Linearised variation model
def variation_model(t, y, u_base):
    du, dup = y
    cosh_t = np.cosh(t)
    sinh_t = np.sinh(t)
    rho_val = 1 + beta * u_base
    return np.vstack((
        dup,
        (F_prime(u_base) * du / cosh_t**2
         - omega * beta * sinh_t / (cosh_t**3 * np.sqrt(rho_val)) * du
         - (omega**2 * beta * sinh_t**2) / (2 * cosh_t**4) * du)
    ))


def bc(ya, yb): return np.array([ya[0], yb[0]])
t1, t2 = 0, 1
t_init = np.linspace(t1, t2, 200)
u_guess = 0.1 * np.sin(np.pi * (t_init - t1) / (t2 - t1))
du_guess = 0.1 * (np.pi / (t2 - t1)) * np.cos(np.pi * (t_init - t1) / (t2 - t1))
y_guess = np.vstack((u_guess, du_guess))
```

```
# Solve base system
sol = solve_bvp(acc_model, bc, t_init, y_guess)
t_fine = np.linspace(t1, t2, 400)
u_base = sol.sol(t_fine)[0]

# Solve variation system
def linearised_system(t, y): return variation_model(t, y, sol.sol(t)[0])
y0_var = np.vstack((0.01 * np.sin(np.pi * t_fine), 0.0 * t_fine))
sol_var = solve_bvp(linearised_system, bc, t_fine, y0_var)
du_sol = sol_var.sol(t_fine)[0]

# Plot
plt.figure(figsize=(8, 5))
plt.plot(t_fine, du_sol, label=r'$\delta u(t)$')
plt.axhline(0, color='grey', linestyle='--', linewidth=0.8)
plt.title('Linearised Stability Test')
plt.xlabel(r'$t$')
plt.ylabel(r'$\delta u(t)$')
plt.grid(True)
plt.legend()
plt.tight_layout()
plt.show()
```

A.3. Python Code for Numerical/Analytic Comparison

```
import numpy as np
import matplotlib.pyplot as plt
from scipy.integrate import solve_bvp

omega = 4650
beta = 0.005

def F(u): return 100
def rho(u): return 1
def rho_prime(u): return 0

def acc_model(t, y):
    u, up = y
    cosh_t = np.cosh(t)
    sinh_t = np.sinh(t)
    u_double_prime = (
        F(u) / cosh_t**2
        - 2 * omega * sinh_t / cosh_t**3
    )
    return np.vstack((up, u_double_prime))


def bc(ya, yb): return np.array([ya[0], yb[0]])


t1, t2 = 0, 1
t_init = np.linspace(t1, t2, 100)
u_guess = 0.01 * np.sin(np.pi * (t_init - t1) / (t2 - t1))
du_guess = 0.01 * (np.pi / (t2 - t1)) * np.cos(np.pi * (t_init - t1) / (t2 - t1))
y_guess = np.vstack((u_guess, du_guess))
```

```python
solution = solve_bvp(acc_model, bc, t_init, y_guess)

# Sample grid
t_fine = np.linspace(t1, t2, 500)
t_sample = np.linspace(t1, t2, 25)

# Numerical solution (interpolated at t_sample)
u_num_sample = solution.sol(t_sample)[0]

# Analytic solution (full line)
def u_analytic(t):
    return 100 * (np.log(np.cosh(t)) - t * np.log(np.cosh(1))) + \
            4650 * (np.tanh(t) - t * np.tanh(1))

u_ana_line = u_analytic(t_fine)

# Plot
plt.figure(figsize=(8, 5))
plt.plot(t_fine, u_ana_line, label='Analytic', linewidth=2)
plt.plot(t_sample, u_num_sample, 'o', label='Numerical', color='red')
plt.title('Analytic vs Numerical Solution of ACC Model')
plt.xlabel(r'$t$')
plt.ylabel(r'$u(t)$')
plt.grid(True)
plt.legend()
plt.tight_layout()
plt.show()

print("   t    | Numerical      | Analytic      ")
print("-----------------------------------------")
for t_val, u_num in zip(t_sample, u_num_sample):
    u_ana = u_analytic(t_val)
    print(f"{t_val:7.4f} | {u_num:14.8f} | {u_ana:14.8f}")
```

A.4. Python Code for Different Functions $\rho(u)$

```python
import numpy as np
import matplotlib.pyplot as plt
from scipy.integrate import solve_bvp

omega = 4650
beta = 0.005

def F(u): return -u

def rho_const(u): return 1 * np.ones_like(u)
def rho_linear(u): return 1 + beta * u
def rho_quadratic(u): return 1 + beta * u**2
def rho_tanh(u): return 1 + np.tanh(beta * u)
def rho_exp(u): return np.exp(beta * u)

def prime_rho_const(u): return np.zeros_like(u)
def prime_rho_linear(u): return beta * np.ones_like(u)
def prime_rho_quadratic(u): return 2 * beta * u
def prime_rho_tanh(u): return beta * (1 - np.tanh(beta * u)**2)
```

```python
def prime_rho_exp(u): return beta * np.exp(beta * u)

def acc_model_generator(rho_func, rho_prime_func):
    def acc_model(t, y):
        u, up = y
        cosh_t = np.cosh(t)
        sinh_t = np.sinh(t)
        rho_val = rho_func(u)
        drho_val = rho_prime_func(u)
        F_val = F(u)
        u_double_prime = (
            F_val / cosh_t**2
            - 2 * omega * np.sqrt(rho_val) * sinh_t / cosh_t**3
            - omega**2 * drho_val * sinh_t**2 / (2 * cosh_t**4)
        )
        return np.vstack((up, u_double_prime))
    return acc_model


def bc(ya, yb): return np.array([ya[0], yb[0]])

t1, t2 = 0, 1
t_init = np.linspace(t1, t2, 100)
u_guess = 0.01 * np.sin(np.pi * (t_init - t1) / (t2 - t1))
du_guess = 0.01 * (np.pi / (t2 - t1)) * np.cos(np.pi * (t_init - t1) / (t2 - t1))
y_guess = np.vstack((u_guess, du_guess))


different_rho = [
    (rho_const, prime_rho_const, r"$\rho = 1$"),
    (rho_linear, prime_rho_linear, r"$\rho = 1 + \beta u$"),
    (rho_quadratic, prime_rho_quadratic, r"$\rho = 1 + \beta u^2$"),
    (rho_tanh, prime_rho_tanh, r"$\rho = 1 + \tanh(\beta u)$"),
    (rho_exp, prime_rho_exp, r"$\rho = e^{\beta u}$")
]


t_fine = np.linspace(t1, t2, 100)
fig, ax = plt.subplots(figsize=(10, 6), dpi=150)
for rho_func, rho_prime_func, label in different_rho:
    model = acc_model_generator(rho_func, rho_prime_func)
    sol = solve_bvp(model, bc, t_init, y_guess, tol=1e-4, max_nodes=10000)
    print("Success:", sol.success)
    ax.plot(t_fine, sol.sol(t_fine)[0], label=label)


ax.set_title("ACC Model: Different $\\rho(u)$ with $F(u) = 1000$")
ax.set_xlabel("$t$")
ax.set_ylabel("$u(t)$")
ax.legend()
ax.grid(True)
plt.tight_layout()
plt.show()
```

Bibliography

[1] Luca Bonaventura, Roberta Ferretti, Andreas Dedner, and Dietmar Kröner. Multilayer shallow water models with locally variable number of layers and semi-implicit time discretization. *Journal of Computational Physics*, 366:15–34, 2018. doi: 10.1016/j.jcp.2018.03.017.

[2] J. Chu. On a nonlinear model for arctic gyres. *Annali di Matematica Pura ed Applicata*, 197(2):651–659, 2018. doi: 10.1007/s10231-017-0696-6.

[3] J. Chu and K. Marynets. Nonlinear differential equations modeling the antarctic circumpolar current. *Journal of Mathematical Fluid Mechanics*, 23(4):1–9, 2021. doi: 10.1007/s00021-021-00618-7.

[4] A. Constantin and R. S. Johnson. Large gyres as a shallow-water asymptotic solution of euler's equation in spherical coordinates. *Proceedings of the Royal Society A: Mathematical, Physical and Engineering Sciences*, 473(2202):20170063, 2017. doi: 10.1098/rspa.2017.0063.

[5] Q. Ding, F.-f. Liao, and S. Wang. Existence, uniqueness and stability for a nonlinear problem arising from stratified arctic gyres. *Annali di Matematica Pura ed Applicata*, 2023. doi: 10.1007/s10231-023-01411-1.

[6] Gelogia. Types of oceanic gyres, 2024. URL https://gelogia.com/types-of-oceanic-gyres/. Accessed: 18-06-2025.

[7] S. Haziot. Study of an elliptic partial differential equation modelling the antarctic circumpolar current. *Discrete and Continuous Dynamical Systems*, 39(8):4415–4427, 2019. doi: 10.3934/dcds.2019188.

[8] K. Marynets. Existence of solutions to a nonlinear elliptic equation modelling large-scale ocean flows. *Monatshefte für Mathematik*, 184(3):419–427, 2017. doi: 10.1007/s00605-016-1002-6.

[9] K. Marynets. A weighted sturm–liouville problem related to ocean flows. *Journal of Mathematical Fluid Mechanics*, 20(3):929–935, 2018. doi: 10.1007/s00021-017-0347-0.

[10] K. Marynets. A nonlinear two-point boundary-value problem in geophysics. *Monatshefte für Mathematik*, 188(2):287–295, 2019. doi: 10.1007/s00605-017-1127-x.

[11] National Ocean Service, NOAA. Surface ocean currents, 2024. URL https://oceanservice.noaa.gov/education/tutorial_currents/04currents1.html. Accessed: June 5, 2025.

[12] Y.-H. Park, T. Park, T.-W. Kim, S.-H. Lee, C.-S. Hong, J.-H. Lee, et al. Observations of the antarctic circumpolar current over the udintsev fracture zone, the narrowest choke point in the southern ocean. *Journal of Geophysical Research: Oceans*, 124:4511–4528, 2019. doi: 10.1029/2019JC015024. URL https://doi.org/10.1029/2019JC015024. Accessed online via AGU Library.

[13] S. R. Rintoul, C. W. Hughes, and D. Olbers. The antarctic circumpolar current system. In G. Siedler, J. Church, and J. Gould, editors, *Ocean Circulation and Climate*, pages 271–302. Academic Press, 2001.

[14] United Nations. Chapter 36h: The southern ocean. https://www.un.org/depts/los/global_reporting/WOA_RPROC/Chapter_36H.pdf, 2021. In: The Second World Ocean Assessment.

[15] G.-K. Vallis. *Atmospheric and Oceanic Fluid Dynamics*. Cambridge University Press, 2006.

[16] G.-K. Vallis. *Geophysical Fluid Dynamics*. Elsevier, 2nd edition, 2019. URL https://www.sciencedirect.com/book/9780128225769/geophysical-fluid-dynamics. Accessed online via ScienceDirect.

[17] Wikipedia contributors. Earth's rotation. https://en.wikipedia.org/wiki/Earth%27s_rotation, 2024. Accessed: 2025-06-16.

[18] Wikipedia contributors. Ocean gyre — wikipedia, the free encyclopedia, 2024. URL `https://en.wikipedia.org/wiki/Ocean_gyre`. Accessed: 17 June 2025.

[19] Wikipedia contributors. Schauder fixed-point theorem — Wikipedia, the free encyclopedia, 2024. URL `https://en.wikipedia.org/wiki/Schauder_fixed-point_theorem`. Accessed: 2025-06-18.

[20] Wikipedia contributors. Arzelà–ascoli theorem — wikipedia, the free encyclopedia, 2024. URL `https://en.wikipedia.org/wiki/Arzel%C3%A0%E2%80%93Ascoli_theorem`. Accessed: 2025-06-17.